SIMULTANEOUS LAYOUT AND DEVICE PARAMETER OPTIMISATION OF A WAVE ENERGY PARK IN AN IRREGULAR SEA

A PREPRINT

Ben Wilks[1*]**, Michael H. Meylan**[1]**, Fabien Montiel**[2]**, Dasun Shalila Balasooriya**[1]**, Tahir Jauhar**[3]**,
Craig Wheeler**[3] **& Stephan Chalup**[1]

1. School of Information and Physical Sciences, University of Newcastle, Callaghan NSW 2308, Australia

2. Department of Mathematics and Statistics, University of Otago, Dunedin 9016, New Zealand

3. School of Engineering, University of Newcastle, Callaghan NSW 2308, Australia

* Email for correspondence: ben.wilks@newcastle.edu.au

ABSTRACT

The design of optimal wave energy parks, namely, arrays of devices known as wave energy converters (WECs) that extract energy from water waves, is an important consideration for the renewable transition. In this paper, the problem of simultaneously optimising the layout and device parameters of a wave energy park is considered within the framework of linear water wave theory. Each WEC is modelled as a heaving truncated cylinder coupled to a spring-damper power take-off. The single-WEC scattering problem is solved using an integral equation/Galerkin method, and interactions between the WECs are solved via a self-consistent multiple scattering theory. The layout of the array and power take-off parameters of its constituent devices are simultaneously optimised using a genetic algorithm, with the goal of maximising energy absorption under a unidirectional, irregular sea described by a Pierson–Moskowitz spectrum. When constrained to a rectangular bounding box that is elongated in the direction of wave propagation, the optimal arrays consist of graded pseudo-line arrays when the number of WECs is sufficiently large. Moreover, low-frequency waves propagate further into the array than high-frequency waves, which is indicative of rainbow absorption, namely, the effect wherein waves spatially separate in a graded array based on their frequency, and are preferentially absorbed at these locations. Arrays optimised for a square bounding box did not show strong evidence of grading or rainbow reflection, which indicates that more complicated interaction effects are present.

1 Introduction

The development of technologies to harness the energy of ocean waves is an important avenue of research for the renewable transition, as the large amount of energy contained in ocean waves makes them an attractive resource [Guo and Ringwood, 2021]. To date, the existing technology for ocean wave energy conversion is not as economically efficient as wind or solar energy conversion, preventing widespread adoption. To address this, the main approach has been to improve the design of energy-harnessing devices, commonly referred to as wave energy converters [WECs, Falnes, 2007, de O. Falcão, 2010, Sheng, 2019]. This paper considers a secondary approach, which is to optimise the configurations of arrays of WEC, known as wave energy parks [Göteman et al., 2020, Teixeira-Duarte et al., 2022, Golbaz et al., 2022].

Optimisation of wave energy parks is a challenging computational task. Simulating wave interactions with the park is expensive, and optimisation becomes more expensive as the number of WECs increases, as the number of WECs determines the number of variables to be optimised. Previous approaches have simplified the task by fixing the device parameters during optimisation, allowing only the park layout to vary. Child and Venugopal [2010] optimised the layout of an array of cylindrical WECs for maximum power take-off in a regular sea, using both a genetic algorithm and a parabolic intersection method. The parameters of the device were optimised prior to the layout optimisation. Using the same algorithms, McGuinness [2018] considered several layout optimisation problems for arrays of point absorbers, including line arrays, circular arrays, and arbitrary layouts. The more realistic problem of optimising the array for an

irregular sea was considered by Child [2011] and McGuinness [2018], in which the sea state was described by the JONSWAP spectrum in both studies. Giassi and Göteman [2018] used a genetic algorithm to optimise an array for absorption from an irregular sea described by time-series data from a site in Sweden. Neshat et al. [2020] considered the problem of optimising an array of submerged three-tether buoys in irregular seas described using observational data taken from sites near Australian cities. In this study, the directional spectrum of the incident waves was also considered. The problem of optimising for irregular sea conditions is more computationally challenging because the underlying wave-park interaction model has to be evaluated across a range of frequencies, making objective function evaluation more expensive. Our task in this paper is to simultaneously optimise the layout and device parameters of the park—we are not aware of any similar work. In particular, the parameters of the park will be tuned in order to maximise power take-off from an irregular sea. In addition to maximising power take-off, previous work has considered secondary objectives, such as minimising installation and maintenance costs of the associated electrical infrastructure of the park [Arbonès et al., 2018, Bergström and Göteman, 2024], using multiple objective optimisation. This is outside the scope of the current paper.

A promising concept to advance wave energy park optimisation is rainbow absorption. This phenomenon, which arises from the field of metamaterials, occurs when waves propagate through an array with graded, locally resonant properties. The graded structure causes the wave energy to gradually slow down and amplify in a location that depends on its frequency, before being absorbed through a loss mechanism. Following earlier investigations in the context of acoustics [Jiménez et al., 2017] and elasticity [Chaplain et al., 2020a], rainbow absorption has since been studied in water waves. Wilks et al. [2022] considered a device consisting of multiple surface-piercing vertical barriers with a graded submergence depth in a two-dimensional fluid, which slows down and spatially separates incident energy into different regions. Rainbow absorption was induced by a loss mechanism consisting of rectangular pistons between each adjacent pair of barriers, which were coupled to a linear power take-off system. When optimised using a local search algorithm, the resulting device achieved near-perfect energy absorption over a prescribed frequency interval (more than 98% of the energy absorbed). Westcott et al. [2024] achieved near-perfect energy absorption by an array of rectangular WECs in the absence of a surrounding structure (i.e. barriers) by using springs to tune the resonances of the WECs and therefore the grading of the array. The WEC parameters that achieved this were found using a two-stage local search optimisation procedure, by first tuning the spring stiffness coefficients to achieve near-perfect reflection by the array and then tuning the power take-off parameters for near-perfect absorption. In these aforementioned studies of rainbow absorption, the grading of the device was imposed as a constraint in the optimisation procedure. While this assumption is sufficient to achieve near-perfect energy absorption in a two-dimensional context, it is unclear whether (and under what conditions) grading would be optimal in a more realistic three-dimensional model. This paper addresses this question by optimising a three-dimensional wave energy farm in the absence of any *a priori* assumption of grading.

The outline of this paper is as follows. In §2 we introduce a model of a WEC that consists of a truncated, partially submerged cylinder, which is constrained to move in heave and coupled to a spring-damper system. Solutions to the single- and multiple-scattering problems are then described, and details of the array power take-off calculations used later in the paper are given. In §3, the constrained optimisation problem for the array is stated, in which both the coordinates and the spring-damper parameters of the WECs are variables. Optimally configured arrays and their absorption spectra, which we find using a genetic algorithm, are given in §4. A discussion is given in §5.

2 Problem formulation and solution

2.1 Scattering by a single WEC

We initially consider a single WEC consisting of a truncated cylinder partially submerged in a fluid of constant depth H. The WEC is constrained to move in heave and coupled to a power take-off mechanism that we model as a linear spring-damper system. The problem is initially posed in a Cartesian coordinate system, in which the xy-plane coincides with the undisturbed free surface of the fluid and the z axis, which points vertically upwards, coincides with the central axis of the WEC. With the intention of applying the method of separation of variables, the system is transformed into cylindrical coordinates (r, θ, z) in which $x = r\cos\theta$ and $y = r\sin\theta$. A scattering problem in the fluid is posed using time-harmonic linear water wave theory, which assumes that the fluid is incompressible and inviscid and undergoing irrotational, time-harmonic motion with time dependence $\mathrm{e}^{-\mathrm{i}\omega t}$ [Linton and McIver, 2001, Mei et al., 2005]. Under these assumptions, the problem reduces to finding the complex potential ϕ, which satisfies the following boundary
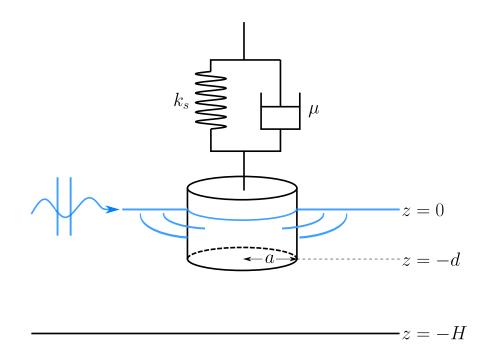
Figure 1: Schematic of the cylindrical WEC model considered in this paper. The radius and equilibrium submergence of the cylinder are denoted a and d, respectively, and the fluid is of constant depth H. An incident wave excites the WEC into vertical motion, which drives an external spring-damper system (with spring and damping coefficients k_s and μ, respectively) and also generates scattered waves in the fluid.

value problem:

$$\triangle\phi = 0 \qquad\qquad (r,\theta,z) \in \Omega \qquad\qquad (1a)$$

$$\partial_z\phi = -\mathrm{i}\omega s \qquad\qquad r < a, z = -d \qquad\qquad (1b)$$

$$\partial_z\phi = \frac{\omega^2}{g}\phi \qquad\qquad r > a, z = 0 \qquad\qquad (1c)$$

$$\partial_z\phi = 0 \qquad\qquad z = -H \qquad\qquad (1d)$$

$$\partial_r\phi = 0 \qquad\qquad r = a, z > -d, \qquad\qquad (1e)$$

where Ω is the fluid domain, g is acceleration due to gravity, a and d are the radius and equilibrium submergence of the cylinder and s is its heave amplitude, which is assumed to be small. Equations (1) are solved in conjunction with a prescribed incident wave, a Sommerfeld radiation condition as $r \to \infty$, a cube-root singularity condition at the submerged edge of the cylinder, and a frequency-domain equation of motion of the WEC, which is given as

$$-\omega^2\rho d\pi a^2 s = \mathrm{i}\omega\mu s - k_s s - \rho g\pi a^2 s + \mathrm{i}\omega\rho \int_{-\pi}^{\pi}\int_0^a \phi(r,\theta,-d)r\mathrm{d}r\mathrm{d}\theta. \qquad (2)$$

The terms on the right hand side of the above equation correspond to the damping, spring, hydrostatic and hydrodynamic forces, respectively, with ρ, μ and k_s being the fluid density, damping coefficient and spring coefficient, respectively. By rotational symmetry, the solution to (1) can be expressed as

$$\phi(r,\theta,z) = \sum_{n=-\infty}^{\infty} \phi_n(r,z)\mathrm{e}^{\mathrm{i}n\theta} \qquad (3)$$

where the functions ϕ_n have a piecewise definition depending on whether a point (r,z) is beneath the WEC (i.e., $r < a$) or not (i.e., $r > a$), that is

$$\phi_n(r,z) = \begin{cases} \varphi_n(r,z) & r > a, \quad z \in (-H,0) \\ \chi_n(r,z) & r < a, \quad z \in (-H,-d). \end{cases} \qquad (4)$$

3

Simultaneous layout and device parameter optimisation of a wave energy park in an irregular sea

The functions φ_n and χ_n are obtained using separation of variables as

$$\varphi_n(r,z) = \sum_{m=0}^{\infty} \psi_m(z) \left(A_{mn} \frac{J_n(k_m r)}{J_n'(k_m a)} + B_{mn} \frac{H_n^{(1)}(k_m r)}{H_n^{(1)\prime}(k_m a)} \right) \tag{5a}$$

$$\chi_n(r,z) = \begin{cases} C_{0n} \frac{r^{|n|}}{|n| a^{|n|-1}} + \sum_{m=1}^{\infty} \tilde{\psi}_m(z) C_{mn} \frac{I_n(\kappa_m r)}{I_n'(\kappa_m a)} & n \neq 0 \\ C_{00} + \sum_{m=1}^{\infty} \tilde{\psi}_m(z) C_{m0} \frac{I_0(\kappa_m r)}{I_0'(\kappa_m a)} - \frac{i\omega s}{2h} \left((z+H)^2 - \frac{r^2}{2} \right) & n = 0 \end{cases} \tag{5b}$$

where J_n, $H_n^{(1)}$ and I_n denote the Bessel, Hankel and modified Bessel functions of the first kind of order n, respectively. The quantities k_m are the solutions to the dispersion relation $k \tanh(kH) = \omega^2/g$, with $k_0 \in \mathbb{R}^+$ being the wavenumber associated with propagating waves. Additionally, $\kappa_m = m\pi/h$, where $h = H - d$. The vertical eigenfunctions are given by $\psi_m(z) = \beta_m^{-1/2} \cosh(k_m(z+H))$, where $\beta_m = \sinh(2k_m H)/4k_m H + \frac{1}{2}$, and $\tilde{\psi}_m(z) = \sqrt{2} \cos(\kappa_m(z+H))$. The term proportional to s in (5b) is a particular solution for the inhomogeneous boundary condition (1b) [Yeung, 1981].

Equation (4) gives rise to a matching problem for each n between the interior region $r < a$ and the exterior region $r > a$, as ϕ_n must be continuously differentiable at $r = a$, namely

$$\varphi_n(a,z) = \chi_n(a,z) \tag{6a}$$

$$\partial_r \varphi_n(a,z) = \partial_r \chi_n(a,z), \tag{6b}$$

for $z \in (-H, -d)$. It follows that the matching problem for a given n is to determine the coefficients B_{mn} and C_{mn} in terms of the coefficients A_{mn}, which are characterised by a known incident wave. The matching problem for ϕ_0 must be solved in tandem with the equation of motion (2), and the WEC heave amplitude s is determined from this problem alone. Conversely, for $n \neq 0$, the modes ϕ_n are uncoupled from the motion of the WEC, and are equivalent to the modes of diffraction around a fixed cylinder.

2.2 Solution using an integral equation/Galerkin method

While early solutions of problems of wave scattering by truncated cylinders used the eigenfunction matching method [Garrett, 1971, Yeung, 1981], here we follow Li and Liu [2019] and use a singularity respecting integral equation/Galerkin method. Such methods typically provide more accuracy for the same computing time [Wilks and Meylan, 2025]. Although we require the solution to the matching problem (6) for all n is solved, here we only show the calculation for the case when $n = 0$, as this is the mode which is coupled to the WEC dynamics. The cases for $n \neq 0$ are similar, though importantly they are independent of the vertical motion of the WEC. More complete explanations of the method are given by Porter [1995] and Kanoria et al. [1999].

The condition that $\partial_r \phi_0$ is continuous at $r = a$ (6b), together with (1e), gives

$$u(z) = \partial_r \varphi_0(a,z) = \begin{cases} 0 & z > -d \\ \partial_r \chi_0(a,z) & z < -d, \end{cases} \tag{7}$$

where we have introduced an auxiliary function u. In terms of the eigenfunction expansions, we have

$$u(z) = \sum_{m=0}^{\infty} \psi_m(z)(A_{m0} + B_{m0}) \tag{8a}$$

$$= \frac{i\omega s a}{2h} + \sum_{m=1}^{\infty} \tilde{\psi}_m(z) C_{m0}. \tag{8b}$$

Using the orthogonality of the vertical eigenfunctions, namely

$$\int_{-H}^{0} \psi_m(z)\psi_n(z)\mathrm{d}z = H\delta_{mn} \quad \text{and} \quad \int_{-H}^{-d} \tilde{\psi}_m(z)\tilde{\psi}_n(z)\mathrm{d}z = h\delta_{mn}, \tag{9}$$

the following expressions for the unknown coefficients are obtained in terms of u:

$$B_{m0} = \frac{1}{H} \int_{-H}^{-d} \psi_m(\xi) u(\xi) \mathrm{d}\xi - A_{m0} \qquad\qquad m \geq 0 \tag{10a}$$

$$C_{m0} = \frac{1}{h} \int_{-H}^{-d} \tilde{\psi}_m(\xi) u(\xi) \mathrm{d}\xi \qquad\qquad m > 0. \tag{10b}$$

4

Note that in (10b), there is no dependence on s since

$$\int_{-H}^{-d} \tilde{\psi}_m(z)\mathrm{d}z = 0, \tag{11}$$

for all $m > 0$. The requirement that ϕ_0 itself is also continuous at $r = a$ (6a), combined with the expressions for the coefficients (10), eventually gives rise to the following integral equation:

$$\int_{-H}^{-d} \mathcal{K}(z,\xi)u(\xi)\mathrm{d}\xi + C_{00} - \frac{\mathrm{i}\omega s}{2h}\left((z+H)^2 - \frac{a^2}{2}\right) = \mathcal{F}(z), \tag{12}$$

where

$$\mathcal{K} = \frac{1}{h}\sum_{m=1}^{\infty}\frac{I_0(\kappa_m a)}{I_0'(\kappa_m a)}\tilde{\psi}_m(z)\tilde{\psi}_m(\xi) - \frac{1}{H}\sum_{m=0}^{\infty}\frac{H_0^{(1)}(k_m a)}{H_0^{(1)'}(k_m a)}\psi_m(z)\psi_m(\xi)$$

$$\mathcal{F}(z) = \sum_{m=0}^{\infty} A_{m0}\left(\frac{J_0(k_m a)}{J_0'(k_m a)} - \frac{H_0^{(1)}(k_m a)}{H_0^{(1)'}(k_m a)}\right)\psi_m(z).$$

To obtain a numerical solution of the integral equation (12), the auxiliary function is expanded in a specified basis as

$$u(z) = \sum_{j=0}^{N_{\mathrm{aux}}} c_j v_j(z), \tag{13}$$

where N_{aux} is a truncation parameter. Substituting this expression into (12) and imposing Galerkin orthogonality (i.e., the residual error is orthogonal to the basis functions v_p for $0 \leq p \leq N_{\mathrm{aux}}$) gives a system of $N_{\mathrm{aux}} + 1$ equations and $N_{\mathrm{aux}} + 3$ unknowns—these being the auxiliary coefficients c_j, the coefficient C_{00} and the piston amplitude s. In order to determine the system, two additional equations are required. The first equation is obtained by integrating (8b) over $(-H, -d)$, giving

$$\int_{-H}^{-d} u(\xi)\mathrm{d}\xi = \frac{\mathrm{i}\omega sa}{2}, \tag{14}$$

where the left hand side can be expressed in terms of the auxiliary coefficients c_j. The second equation is provided by the equation of motion (2), where we note that the integral on the right hand side is independent of ϕ_n for $n \neq 0$, since the terms $e^{\mathrm{i}n\theta}$ integrate to zero.

The resulting system of equations has a matrix representation of the form

$$\begin{bmatrix} K & \boldsymbol{\gamma}^1 & -\boldsymbol{\gamma}^2 \\ (\boldsymbol{\gamma}^1)^{\mathsf{T}} & 0 & -\mathrm{i}\omega a/2 \\ (\boldsymbol{\gamma}^3)^{\mathsf{T}} & \mathrm{i}\omega\rho\pi a^2 & \Box \end{bmatrix} \begin{bmatrix} \mathbf{c} \\ C_{00} \\ s \end{bmatrix} = \begin{bmatrix} \mathbf{F} \\ 0 \\ 0 \end{bmatrix} \tag{15}$$

where the $N_{\mathrm{aux}} + 1$-dimensional matrix K and vectors $\boldsymbol{\gamma}^1$, $\boldsymbol{\gamma}^2$ and $\mathbf{F}$ are derived from the integral equation (12) and Galerkin orthogonality, and have entries

$$K_{pj} = \int_{-H}^{-d}\int_{-H}^{-d} v_z(\xi)\mathcal{K}(z,\xi)v_j(\xi)\mathrm{d}\xi\mathrm{d}z \tag{16a}$$

$$\gamma_1^p = \int_{-H}^{-d} v_p(z)\mathrm{d}z \tag{16b}$$

$$\gamma_p^2 = \frac{-\mathrm{i}\omega}{2h}\int_{-H}^{-d}\left((z+H)^2 - \frac{a^2}{2}\right)v_p(z)\mathrm{d}z \tag{16c}$$

$$F_p = \int_{-H}^{-d} \mathcal{F}(z)v_p(z)\mathrm{d}z, \tag{16d}$$

where we note that F_p depends linearly on the incident wave coefficients A_{m0}. The entries of the vector $\mathbf{c}$ are the auxiliary coefficients c_j. The second row of the matrix expression (15) is derived from (14), and the third row is derived from the equation of motion (2). For brevity, the entries of the $N_{\mathrm{aux}} + 1$-dimensional vector $\boldsymbol{\gamma}^3$ are not stated—we merely note that they express the dependence of the integral in (2) on the auxiliary coefficients c_j via the coefficients C_{m0}, for $m \geq 1$. The number $\Box$ is the only element of the matrix in (15) which depends on the WEC spring-damper

properties k_s and μ. If the radius a and depth d are held fixed, the remaining entries of the matrix in (15) can be precomputed, which rapidly accelerates computation. Once the system in (15) is solved, the scattered wave coefficients B_{m0} are readily obtained from the auxiliary coefficients c_j.

In order to capture the cube root singularity of $\nabla\phi_n$ at the submerged corner $(r, z) = (a, -d)$, the auxiliary basis is taken to consist of weighted Gegenbauer polynomials of the form [Kanoria et al., 1999]

$$v_j(z) = \frac{2^{7/6}\Gamma(1/6)(2j)!}{\pi\Gamma(2j + 1/3)h^{1/3}}(h^2 - (z + H)^2)^{-1/3}C_{2m}^{1/6}\left(\frac{z + H}{h}\right) \tag{17}$$

2.3 The T-matrix for a WEC

Solutions of the matching problem for a range of n are used to obtain a T-matrix expression of the form

$$\begin{bmatrix} t_{-N_W} & & & & \\ & \ddots & & & \\ & & t_0 & & \\ & & & \ddots & \\ & & & & t_{N_W} \end{bmatrix} \begin{bmatrix} A_{0,-N_W} \\ \vdots \\ A_{0,0} \\ \vdots \\ A_{0,N_W} \end{bmatrix} = \begin{bmatrix} B_{0,-N_W} \\ \vdots \\ B_{0,0} \\ \vdots \\ B_{0,N_W} \end{bmatrix} \tag{18}$$

which relates incident wave amplitudes to scattered wave amplitudes. The truncation parameter N_W is obtained from Wiscombe's formula [Wiscombe, 1980], which empirically describes the number of angular modes required for convergence as a function of the nondimensional WEC radius $k_0 a$. The T-matrix given in (18) is based on the wide spacing approximation, i.e., evanescent modes (terms for $m > 0$ in (5a)) are not included. The underlying assumption of the wide spacing approximation is that a negligible amount of energy is transmitted by evanescent modes between WECs in the subsequent multiple scattering problem. Note that the T-matrix is diagonal due to rotational symmetry. Moreover, the only entry of the T-matrix which depends on the spring and damping coefficients is t_0; provided a and d are fixed, the remaining entries can be precomputed which rapidly accelerates computation.

For subsequent energy absorption calculations, we also require a way of calculating the heave amplitude of the WEC s from the incident coefficients A_{mn}. By linearity, rotational symmetry, and an assumption that incident evanescent modes are negligible in the excitation of the WEC (i.e., the wide spacing approximation) we note that there is a scalar s_{rel} satisfying $s_{\text{rel}}A_{0,0} = s$, although the details of its derivation are not presented here for brevity.

2.4 Scattering by multiple WECs

Next, we consider the multiple scattering problem of N WECs centred at (x_j, y_j) for $1 \leq j \leq N$, each having constant radius a and equilibrium submergence d but with varying spring and damping coefficients $k_{s,j}$ and μ_j, respectively. The exterior field can be written as a superposition of the incident wave and the waves scattered by all WECs as [Martin, 2006]

$$\phi \approx \phi_{\text{inc}} + \sum_{j=1}^{N} \phi_{\text{sc}}^{(j)}. \tag{19}$$

We approximate the wave scattered by cylinder j using the wide spacing approximation and Wiscombe's truncation formula as

$$\phi_{\text{sc}}^{(j)}(r_j, \theta_j, z) = \psi_0(z) \sum_{n=-N_W}^{N_W} B_{0n}^{(j)} \frac{H_n^{(1)}(k_0 r_j)}{H_n^{(1)\prime}(k_0 a)} e^{\mathrm{i}n\theta}, \tag{20}$$

where (r_j, θ_j, z) are local cylindrical coordinate systems centred at the WEC central axes. They are related to the global cartesian coordinate system by $x = x_j + r_j\cos\theta_j$, and $y = y_j + r_j\sin\theta_j$. The system is solved using the self consistent theory of multiple scattering [Kagemoto and Yue, 1986, Peter and Meylan, 2004, Martin, 2006, Montiel et al., 2024]. The theory results in a system of equations of the form

$$(I - T_{\text{Array}}S_{\text{Array}})\begin{bmatrix} \mathbf{B}^{(1)} \\ \vdots \\ \mathbf{B}^{(N)} \end{bmatrix} = \mathbf{F} \tag{21}$$

where I is the $N(2N_W + 1)$-dimensional identity matrix and the block-diagonal matrix T_{Array} is defined as

$$T_{\text{Array}} = \begin{bmatrix} T^{(1)} & & \\ & \ddots & \\ & & T^{(N)} \end{bmatrix} \tag{22}$$

where $T^{(j)}$ is the T-matrix of the form (18) associated with the jth scatterer. Moreover, S_{Array} is a matrix arising from Graf's addition theorem depending on the frequency and the relative positions of the WECs, but not on their properties. When solving the wave energy park layout optimisation problem described in §3, evaluation of the entries of S_{Array} is one of the most expensive parts of the computation—it cannot be precomputed as the layout varies during the solution procedure. The entries of the vectors $\mathbf{B}^{(j)}$ are $B_{0n}^{(j)}$, i.e., the coefficients of the wave scattered by the jth WEC. Lastly, the forcing vector $\mathbf{F}$ depends on the incident wave ϕ_{inc}. Full details of the derivation of (21) are provided by Martin [2006]. We note that once the scattered wave amplitudes $B_{0n}^{(j)}$ are known, it is straightforward to compute s_j, namely, the complex heave amplitude of each WEC, using quantities analogous to s_{rel} (introduced in §2.3) for each WEC.

2.5   Energy absorption

We consider the array to be subject to irregular plane waves propagating in the positive x direction. Assuming a simple model of a fully developed sea generated by wind-wave interactions, we describe the sea state using the Pierson-Moskowitz spectrum [Pierson Jr and Moskowitz, 1964]

$$S(\omega) = \frac{c_1 g^2}{\omega^5} \exp\left(-\frac{c_2 g^2}{\omega^4 H_s^2}\right) \tag{23}$$

in which $c_1 = 8.1 \times 10^{-3}$ and $c_2 = 3.24 \times 10^{-2}$ are fixed constants and the significant wave height H_s is a free parameter, which we take to be $H_s = 2\,\text{m}$ throughout this paper. The average rate of energy absorption by the array in this sea is given by

$$P_S(\mathbf{X}) = \int_0^\infty P(\mathbf{X}, \omega)\sqrt{2S(\omega)\text{d}\omega}, \tag{24}$$

where $\mathbf{X}$ is a vector containing the parameters of the array, i.e. the coordinates of the WECs and the parameters of their spring-damper systems. The functions $P(\mathbf{X}, \omega)$ represent the average rate of energy absorption by the array when subjected to a unit-amplitude monochromatic plane wave of frequency ω, travelling in the positive x direction. They can be calculated directly from the piston amplitudes as

$$P(\mathbf{X}, \omega) = \sum_{j=1}^N \tfrac{1}{2}\omega^2 \mu_j |s_j|^2 \tag{25}$$

where μ_j and s_j are the damping coefficient and computed amplitude of the jth piston, respectively. The functions $P(\mathbf{X}, \omega)$ can also be calculated at the far field via a generalised optical theorem [Mei et al., 2005]

$$P(\mathbf{X}, \omega) = \omega\rho H \left[\frac{1}{\pi}\int_{-\pi}^{\pi}|\mathcal{B}(\theta)|^2 d\theta - \frac{2\sqrt{\beta_0}g}{\omega\cosh(k_0 H)}\text{Im}(A^*\mathcal{B}(0))\right] \tag{26}$$

where the far field function is defined as

$$\mathcal{B}(\theta) = \sum_{j=1}^N \exp(-\text{i}k_0 R_{0j}\cos(\varphi_{0j} - \theta)) \sum_{n=-\infty}^{\infty} \frac{(-\text{i})^n B_{0n}^{(j)}}{H_n^{(1)\prime}(k_0 a)} e^{\text{i}n\theta}, \tag{27}$$

where (R_{0j}, φ_{0j}) are the polar coordinates of (x_j, y_j) with respect the global polar coordinate system (r, θ). Agreement between (25) and (26), which is equivalent to conservation of energy, is used to validate our computations.

During our numerical computations, the integral in (24) [of which the technical details are discussed in Ochi, 1998] is approximated using the following quadrature rule

$$P_S(\mathbf{X}) \approx \sum_{j=1}^{100} P(\mathbf{X}, \omega_j)\sqrt{2S(\omega_j)\Delta\omega} \tag{28}$$

where $\omega_j = \omega_1 + (j-1)\Delta\omega$ are evenly spaced quadrature points, which are chosen to span an interval over which the spectral density function $S(\omega)$ is non-negligible. In the case where the significant wave height is $H_s = 2\,\text{m}$, the quadrature points are chosen so that $\omega_1 = 0.4\,\text{s}^{-1}$ and $\omega_{100} = 4\,\text{s}^{-1}$ (i.e., wave periods between $1.57\,\text{s}$ and $15.71\,\text{s}$).

3   Optimisation

We set up an optimisation problem that consists in finding $\mathbf{X}_{\text{opt}}$ which maximises the objective function $f(\mathbf{X})$ subject to constraints on the parameters in $\mathbf{X}$. The parameters subject to optimisation are the WEC coordinates (x_j, y_j), and

their spring and damping coefficients $k_{s,j}$ and μ_j, respectively. The objective function $f(\mathbf{X})$ is proportional to $P_S(\mathbf{X})$ except when the distance between any two WECs becomes small—in such situations, a penalty is applied to prevent the assumption of wide spacing from being violated. In particular

$$f(\mathbf{X}) = \begin{cases} f_+(\mathbf{X}) & R_{\min} > 4a \\ \theta f_-(\mathbf{X}) + (1-\theta)f_+(\mathbf{X}) & 3a < R_{\min} < 4a \\ f_-(\mathbf{X}) & R_{\min} < 3a, \end{cases} \tag{29}$$

where $R_{\min} = \min_{i \neq j} R_{ij}$ is the minimum distance between any two pairs of WECs. Moreover, $f_+ = P_S(\mathbf{X})/P_{S,\mathrm{MAX}}$ and $f_- = R_{\min}/(4a) - 1$ are the positive reward and negative penalty functions, respectively, and $\theta = 4 - R_{\min}/a$ is a convex sum parameter. The scalar $P_{S,\mathrm{MAX}}$ is an estimate of the upper bound of the energy absorbed by the array, given by

$$P_{S,\mathrm{MAX}} = N \int_0^\infty \frac{\rho g \omega}{4k_0^2} \left(1 + \frac{2k_0 H}{\sinh(2k_0 H)} \right) \sqrt{2S(\omega)\mathrm{d}\omega}, \tag{30}$$

in which we note that k_0 depends on ω through the dispersion relation. The above estimated bound assumes each WEC is maximally efficient at all frequencies [Mei et al., 2005] and is uncoupled from all other WECs. While we make no attempt to prove that this is an upper bound of $P_S(\mathbf{X})$, we note that it was not exceeded during our computations. The resulting objective function $f(\mathbf{X})$ is expected to be a continuous function of $\mathbf{X}$ taking values in $[-1, 1]$.

For all $1 \leq j \leq N$, the WEC coordinates (x_j, y_j) are constrained to the bounding box $0 \leq x_j \leq D_x$ and $0 \leq y_j \leq D_y$. To simplify computation, we additionally require that (i) $x_1 = 0$ and (ii) $x_1 \leq x_2 \leq ... \leq x_N$. Note that these do not restrict the optimal solutions due to (i) a translation argument and (ii) a permutation argument. Note that condition (i) reduces the number of parameters by 1, meaning that $\mathbf{X}$ is $(4N - 1)$-dimensional. The spring coefficients are restricted to $|k_{s,j}| \leq 10^5 \, \mathrm{kg \, s^{-2}}$. Note that this constraint permits negative spring coefficients, which is not a new idea in wave energy conversion [Zhang et al., 2016, Todalshaug et al., 2016, Têtu et al., 2018, Westcott et al., 2024]. Springs with negative stiffness decrease the resonant frequency of an individual WEC. This could alternatively be achieved by increasing d, i.e., the equilibrium submergence depth of a WEC, although varying k_s is more computationally efficient than varying d because it allows more quantities to be precomputed (as discussed in §2.2). The damping coefficients are restricted to $0 \leq \mu_j \leq 2 \times 10^3 \, \mathrm{kg \, s^{-1}}$. The bounds on $k_{s,j}$ and μ_j are sufficiently non restrictive so that an individual WEC can achieve its theoretical optimal capture width $1/k_0$ across the frequency interval considered in this study $\omega \in [0.4, 4] \, \mathrm{s^{-1}}$. Note that the aforementioned capture width is the length of a wave crest carrying the same amount of energy as the WEC absorbs—the reader is referred to Mei et al. [2005] for further details on this quantity and its theoretical bounds for axisymmetric devices.

The results presented in this paper were obtained using MATLAB's built-in genetic algorithm `ga` with the default settings. A sequential optimisation algorithm motivated by those used in previous studies of rainbow absorption was also considered [Jiménez et al., 2017, Wilks et al., 2022, Westcott et al., 2024], but this yielded poorer optimal solutions than those obtained using the genetic algorithm . Specifically, the sequential algorithm consisted of an iteration, in which each step begins with the optimal array of $N - 1$ WECs, adds a new WEC in a random location to obtain an initial guess $\mathbf{X}_0$, then performs a local search of the parameter space beginning at $\mathbf{X}_0$ using the MATLAB algorithm `fmincon`. As they are better, we only present results obtained using the genetic algorithm in this paper.

4   Results

Figure 2 shows optimised array configurations for a rectangular bounding box $D_x = 200 \, \mathrm{m}$ and $D_y = 50 \, \mathrm{m}$, for an increasing number of WECs. We observe that WECs which are most efficient at higher frequencies occur towards the front of the array, whereas WECs which are most efficient at lower frequencies occur towards the rear of the array. While there does appear to be a grading of the WECs' peak absorption efficiency frequencies across the array, this grading is not monotonic. As the number of WECs N increases, we observe the gradual onset of two parallel pseudo-line arrays approximately along $y = 0 \, \mathrm{m}$ and $y = D_x$. We emphasise that these are not true line arrays as the WECs are not collinear. We hypothesise that these pseudo–line arrays arise in the optimal configurations due to the rainbow absorption effect. In particular, we propose that waves analogous to Rayleigh–Bloch waves propagate along these pseudo-line arrays and gradually slow down as the frequency of the local resonance decreases. The local energy amplification resulting from this subsequently results in efficient absorption. Figure 3 shows the free surface elevation resulting from wave interaction with one of these optimal arrays at four different frequencies. Qualitatively, we observe that lower frequency waves amplify further towards the right of the array, which supports the conclusion that rainbow absorption underpins absorption by this array.

Figure 4 shows the optimised array configurations for a square bounding box $D_x = D_y = 100 \, \mathrm{m}$. While in some cases we observe local grading of the WECs' peak absorption efficiency frequencies, this is not the case globally as
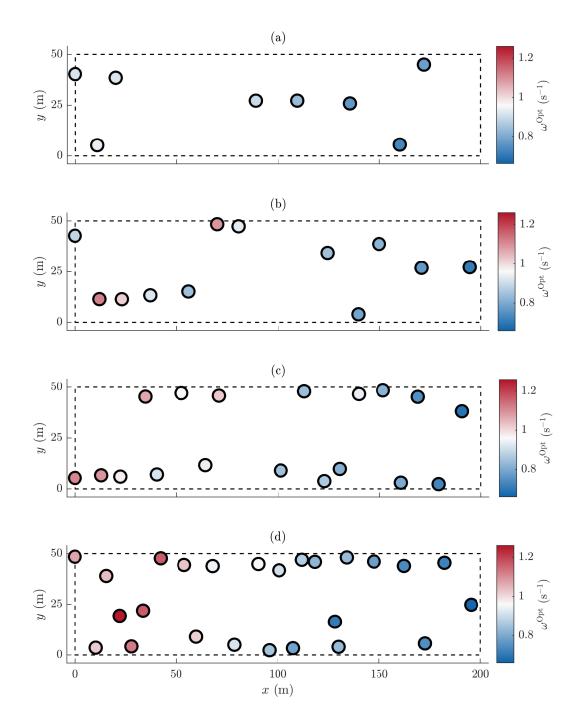
Figure 2: Optimised configurations of an array of (a) $N = 8$, (b) $N = 12$, (c) $N = 18$ and (d) $N = 25$ WECs found using the genetic algorithm, when constrained to a rectangular bounding box $D_x = 200$ m and $D_y = 50$ m (dashed line). The WECs are drawn as circles, whose radii are not drawn to scale. The colour of the WECs indicates ω^{Opt}, i.e. the frequency at which that WEC would optimally absorb energy if uncoupled from all other WECs. The direction of wave propagation is from left to right.
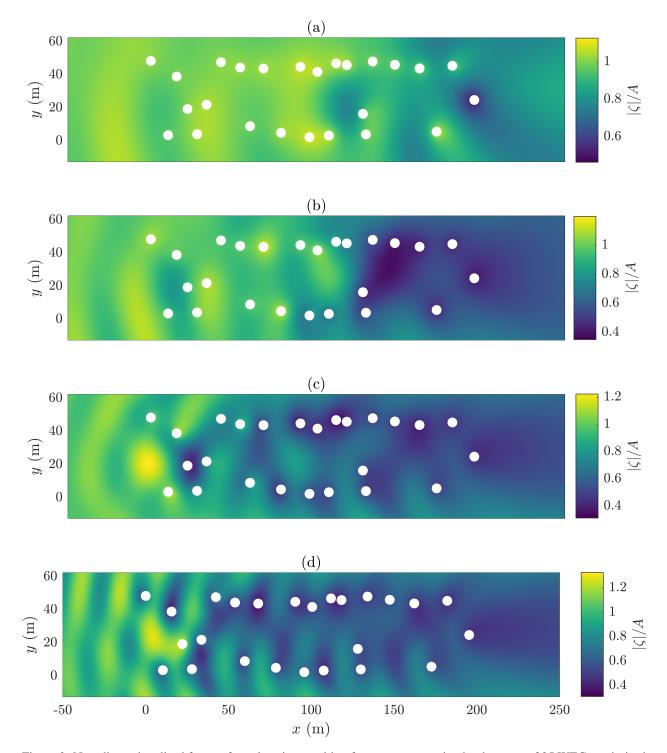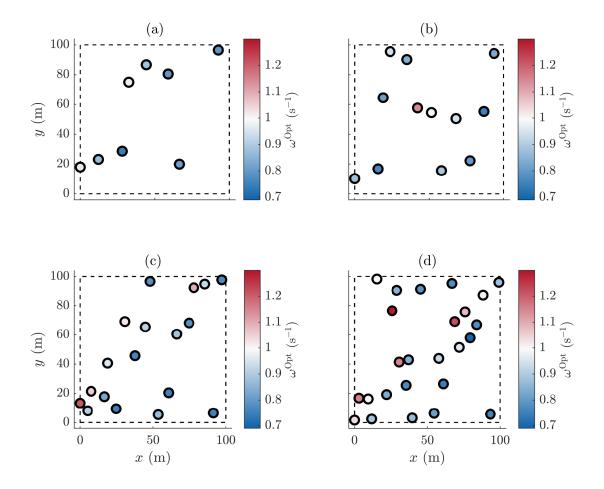
Figure 3: Non-dimensionalised free surface elevation resulting from wave scattering by the array of 25 WECs optimised for the rectangular bounding box $D_x = 200\,\text{m}$ and $D_y = 50\,\text{m}$, at (a) $\omega = 0.7\,\text{s}^{-1}$, (b) $\omega = 0.85\,\text{s}^{-1}$, (c) $\omega = 1\,\text{s}^{-1}$ and (d) $\omega = 1.15\,\text{s}^{-1}$. The WECs are plotted as white circles (not to scale). The non-dimensionalised free surface is defined as $|\zeta(x,y)|/A$, where $\zeta(x,y)$ is the free surface resulting from excitation by a plane wave with amplitude A.

Figure 4: Optimised configurations of an array of (a) $N = 8$, (b) $N = 12$, (c) $N = 18$ and (d) $N = 25$ WECs found using the genetic algorithm, when constrained to a rectangular bounding box $D_x = D_y = 100$ m (dashed line). The WECs are drawn as circles, whose radii are not drawn to scale. The colour of the WECs indicates ω^{Opt}, i.e. the frequency at which that WEC would optimally absorb energy if uncoupled from all other WECs. The direction of wave propagation is from left to right.

the array layouts are very irregular. Thus, interactions between WECs in square-bounded arrays are presumably much more complex than can be understood through the rainbow reflection effect alone. Figure 5 shows the free surface elevation resulting from wave interaction with one of these optimal arrays at four different frequencies. In contrast to the rectangular array in Figure 3, there is little qualitative evidence of rainbow absorption. While there appears to be some indication that low-frequency waves propagate further than high-frequency waves in the panel $y < 30$ m, this is not conclusive. We also remark that square-bounded arrays absorb more energy than rectangle-bounded arrays with the same number of WECs, as shown in Figure 6(a). Presumably, this is because the square bounding box is twice as narrow in the x-direction, meaning that WECs at the rear of the array are subject to weaker shadowing effects.

Because the objective function is not convex, it is important to consider whether the optimal arrays in Figures 2 and 4 are global optima or, if they are only local optima, how significantly they deviate from the global optima. In Figure 7, a histogram is shown for 20 independent realisations of the genetic algorithm in the case $N = 20$, $D_x = 200$ m and $D_y = 50$ m. There is a considerable spread in the range of power take-off values, with the best array outperforming the median by 5%. Thus, the optimal arrays shown in Figures 2 and 4 should only be considered as local optima. We note that a repeated evaluation of the genetic algorithm was not conducted in general in this article due to the computational expense of these evaluations, particularly for large N.

Figure 6 illustrates the effect of the number of WECs N on the power take-off by the optimal arrays. We observe that for both square-bounded and rectangle-bounded arrays, the addition of each successive WEC increases the total power
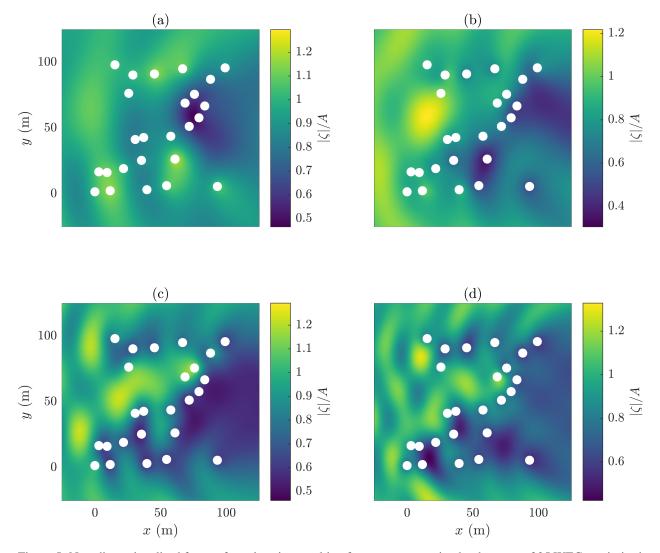
11

Figure 5: Non-dimensionalised free surface elevation resulting from wave scattering by the array of 25 WECs optimised for the square bounding box $D_x = D_y = 100\,\mathrm{m}$, at (a) $\omega = 0.7\,\mathrm{s}^{-1}$, (b) $\omega = 0.85\,\mathrm{s}^{-1}$, (c) $\omega = 1\,\mathrm{s}^{-1}$ and (d) $\omega = 1.15\,\mathrm{s}^{-1}$. The WECs are plotted as white circles (not to scale). The non-dimensionalised free surface is defined as $|\zeta(x,y)|/A$, where $\zeta(x,y)$ is the free surface resulting from excitation by a plane wave with amplitude A.

take-off by the array. However, the rate of power take-off per WEC is predominantly decreasing as a function of N, indicating that there are diminishing returns in adding more WECs to the array.

Figure 8 shows power take-off spectra $P(\mathbf{X}_{\mathrm{opt}}, \omega)$ for the optimal arrays displayed in Figures 2 and 4. Increasing the number of WECs N appears to confer increased power take-off at all frequencies, for both rectangle-bounded and square-bounded arrays. We also observe that the peaks of the power take-off spectra occur at lower frequencies than the peak of the spectral density function $S(\omega)$, presumably because lower frequency waves have a higher group velocity, and therefore transport energy into the array at a higher rate.

5 Discussion

This paper has developed a model of a wave energy park with an arbitrary WEC layout. In the model, each WEC consists of a heaving truncated cylinder that is coupled to a spring-damper system which models power take-off. The layout and device parameters were optimised subject to constraints using a genetic algorithm. The optimisation procedure yielded wave energy park configurations which are local maximisers of energy absorption in a unidirectional, irregular sea. When constrained to a rectangular bounding box that is elongated in the direction of wave propagation, the optimal
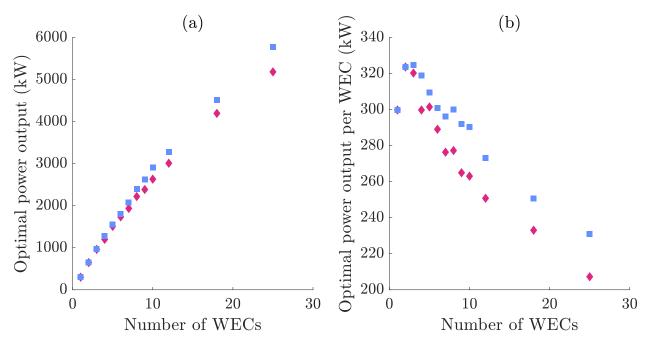
Figure 6: (a) Rate of energy absorption by optimised arrays of WECs $P(\mathbf{X}_\text{opt})$ as a function of the array size N. Values for the rectangular bounding box problem ($D_x = 200\,\text{m}$ and $D_y = 50\,\text{m}$) are marked with magenta diamonds and those for the square bounding box problem ($D_x = D_y = 100\,\text{m}$) are marked with blue squares. (b) As for panel (a), except the vertical axis displays the rate of energy absorption per WEC in the optimised arrays, i.e., $P(\mathbf{X}_\text{opt})/N$.

Figure 7: Histogram showing the rate of energy absorption of optimal arrays found from 20 independent evaluations of the genetic algorithm. Each array consists of 10 WECs bound to the rectangular region ($D_x = 200\,\text{m}$ and $D_y = 50\,\text{m}$).
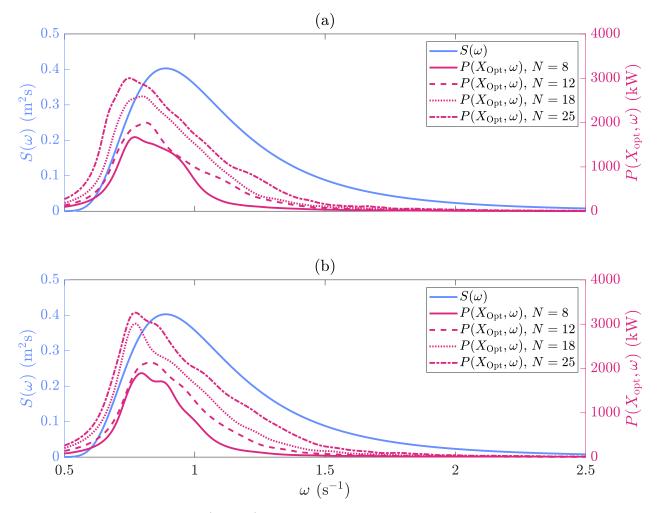
Figure 8: Power take-off spectra $P(\mathbf{X}_{\mathrm{opt}}, \omega)$ for the optimal arrays constrained to the (a) rectangular and (b) square bounding boxes, as displayed in Figures 2 and 4, respectively. The spectral density function $S(\omega)$, which is a Pierson-Moskowitz spectrum with significant wave height $H_s = 2\,\mathrm{m}$, is also shown for comparison.

layout consist of graded pseudo-line arrays when the number of WECs is sufficiently large. Moreover, low-frequency waves propagate further into the array than high-frequency waves, which is indicative of rainbow absorption. Our results were less conclusive in the case of arrays constrained to a square bounding box, where we suspect that phenomena other than rainbow absorption govern the interactions between WECs in the array.

A limitation of this study is the extent to which we have explored the parameter space of our model. One class of parameters that has not been considered is those governing the sea state, namely the significant wave height H_s and the direction of the incident waves. Different choices of these parameters would change the objective function, thereby giving rise to different optimal arrays. While the effect of the sea state on the optimal arrays could be explored using a discrete collection of parameters, a more comprehensive understanding of this effect could be obtained by extending the optimisation problem to a multi-condition problem of the form

$$\min_{\mathbf{X} \in \Omega} f(\mathbf{X}, \mathbf{C}) \quad \text{for all } \mathbf{C} \in \Phi. \tag{31}$$

In the above, Ω is the decision space (here describing the array layout and device parameters) and Φ is the condition space describing parameters which are external to the optimisation problem (here describing the sea state). The task of a multi-condition optimisation problem is to find the optimal solution for all conditions, that is, to find an optimal vector $\mathbf{X}_{\mathbf{C}} \in \Omega$ for all values of $\mathbf{C} \in \Phi$. One avenue for future work is to optimise arrays of WECs using deep reinforcement learning-based algorithms which have recently been proposed for multi-condition optimisation tasks [Kim et al., 2022, Balasooriya et al., 2024].

A second limitation of this work is whether the optimal WEC spring and damping coefficients found in this study are realistic. Future studies could consider what parameter ranges can be engineered in prototype WECs and investigate the array configurations that arise under these restrictions. Another potential weakness is the use of a linearised kinematic condition at the submerged face of each WEC, which can permit unrealistically large heave amplitudes of floating bodies at resonance, particularly when their horizontal extent is much smaller than one wavelength.

Lastly, we mention the important question of whether the irregularity of the optimal arrays, particularly those bounded to the square region, is a feature of optimal arrays or a limitation of the optimisation procedure. In support of the former hypothesis, we tangentially mention the work of Chaplain et al. [2020a], who studied graded arrays of energy-harvesting rods in the context of elastic waves, in which the rods were grouped into triangles in each unit cell. The authors illustrated that the introduction of asymmetry in the unit cell greatly increased the potential for energy harvesting, as it decoupled the wave carrying incident energy into the array from its counterpart carrying reflected energy out of the array. In the same vein, a graded Su–Schrieffer–Heeger metawedge of energy harvesting rods, in which the spacing of the rods is alternating instead of uniform, yielded considerably greater energy amplifications than a conventionally graded structure due to topologically protected edge states [Chaplain et al., 2020b]. In light of these studies, it is perhaps unsurprising that the optimal arrays found in this paper are irregular, although the precise nature of the interaction in these arrays is unknown.

Acknowledgements

References

Dídac Rodríguez Arbonès, Nataliia Y. Sergiienko, Boyin Ding, Oswin Krause, Christian Igel, and Markus Wagner. Sparse incomplete lu-decomposition for wave farm designs under realistic conditions. In Anne Auger, Carlos M. Fonseca, Nuno Lourenço, Penousal Machado, Luís Paquete, and Darrell Whitley, editors, *Parallel Problem Solving from Nature – PPSN XV*, pages 512–524, Cham, 2018. Springer International Publishing. ISBN 978-3-319-99253-2.

Dasun Shalila Balasooriya, Alan Blair, Craig Wheeler, and Stephan Chalup. Multi-condition multi-objective airfoil shape optimisation using deep reinforcement learning compared to genetic algorithms. In *International Conference on Optimization, Learning Algorithms and Applications*, pages 243–258. Springer Nature Switzerland, 2024. doi: https://doi.org/10.1007/978-3-031-77432-4_17.

K Bergström and M Göteman. Comprehensive multi-objective optimisation of wave power parks. In *Innovations in Renewable Energies Offshore*, pages 295–305. CRC Press, 2024. doi: 10.1201/9781003558859-33.

G J Chaplain, Daniel Pajer, Jacopo M De Ponti, and R V Craster. Delineating rainbow reflection and trapping with applications for energy harvesting. *New Journal of Physics*, 22(6):063024, jun 2020a. doi: 10.1088/1367-2630/ab8cae. URL `https://dx.doi.org/10.1088/1367-2630/ab8cae`.

Gregory J. Chaplain, Jacopo M. De Ponti, Giulia Aguzzi, Andrea Colombi, and Richard V. Craster. Topological rainbow trapping for elastic energy harvesting in graded Su-Schrieffer-Heeger Systems. *Phys. Rev. Appl.*, 14: 054035, Nov 2020b. doi: 10.1103/PhysRevApplied.14.054035. URL `https://link.aps.org/doi/10.1103/PhysRevApplied.14.054035`.

Benjamin Frederick Martin Child. *On the configuration of arrays of floating wave energy converters*. PhD thesis, University of Edinburgh, 2011.

B.F.M. Child and V. Venugopal. Optimal configurations of wave energy device arrays. *Ocean Engineering*, 37 (16):1402–1417, 2010. ISSN 0029-8018. doi: https://doi.org/10.1016/j.oceaneng.2010.06.010. URL `https://www.sciencedirect.com/science/article/pii/S0029801810001447`.

António F. de O. Falcão. Wave energy utilization: A review of the technologies. *Renewable and Sustainable Energy Reviews*, 14(3):899–918, 2010. ISSN 1364-0321. doi: https://doi.org/10.1016/j.rser.2009.11.003. URL `https://www.sciencedirect.com/science/article/pii/S1364032109002652`.

Johannes Falnes. A review of wave-energy extraction. *Marine Structures*, 20(4):185–201, 2007. ISSN 0951-8339. doi: https://doi.org/10.1016/j.marstruc.2007.09.001. URL `https://www.sciencedirect.com/science/article/pii/S0951833907000482`.

C. J. R. Garrett. Wave forces on a circular dock. *Journal of Fluid Mechanics*, 46(1):129–139, 1971. doi: 10.1017/S0022112071000430.

Marianna Giassi and Malin Göteman. Layout design of wave energy parks by a genetic algorithm. *Ocean Engineering*, 154:252–261, 2018. ISSN 0029-8018. doi: https://doi.org/10.1016/j.oceaneng.2018.01.096. URL https://www.sciencedirect.com/science/article/pii/S0029801818301045.

Danial Golbaz, Rojin Asadi, Erfan Amini, Hossein Mehdipour, Mahdieh Nasiri, Bahareh Etaati, Seyed Taghi Omid Naeeni, Mehdi Neshat, Seyedali Mirjalili, and Amir H. Gandomi. Layout and design optimization of ocean wave energy converters: A scoping review of state-of-the-art canonical, hybrid, cooperative, and combinatorial optimization methods. *Energy Reports*, 8:15446–15479, 2022. ISSN 2352-4847. doi: https://doi.org/10.1016/j.egyr.2022.10.403. URL https://www.sciencedirect.com/science/article/pii/S235248472202337X.

Malin Göteman, Marianna Giassi, Jens Engström, and Jan Isberg. Advances and challenges in wave energy park optimization—a review. *Frontiers in Energy Research*, 8:26, 2020. doi: 10.3389/fenrg.2020.00026.

Bingyong Guo and John V. Ringwood. A review of wave energy technology from a research and commercial perspective. *IET Renewable Power Generation*, 15(14):3065–3090, 2021. doi: https://doi.org/10.1049/rpg2.12302.

Noé Jiménez, Vicent Romero-García, Vincent Pagneux, and Jean-Philippe Groby. Rainbow-trapping absorbers: Broadband, perfect and asymmetric sound absorption by subwavelength panels for transmission problems. *Scientific reports*, 7(1):1–12, 2017.

Hiroshi Kagemoto and Dick K. P. Yue. Interactions among multiple three-dimensional bodies in water waves: an exact algebraic method. *Journal of Fluid Mechanics*, 166:189–209, 1986. doi: 10.1017/S0022112086000101.

Mridula Kanoria, DP Dolai, and BN Mandal. Water-wave scattering by thick vertical barriers. *Journal of engineering mathematics*, 35:361–384, 1999. doi: 10.1023/A:1004392622976.

Sejin Kim, Innyoung Kim, and Donghyun You. Multi-condition multi-objective optimization using deep reinforcement learning. *Journal of Computational Physics*, 462:111263, 2022. doi: 10.1016/j.jcp.2022.111263.

Ai-jun Li and Yong Liu. New analytical solutions to water wave diffraction by vertical truncated cylinders. *International Journal of Naval Architecture and Ocean Engineering*, 11(2):952–969, 2019. ISSN 2092-6782. doi: 10.1016/j.ijnaoe.2019.04.006.

C. M. Linton and P. McIver. *Handbook of mathematical techniques for wave/structure interactions*. Chapman & Hall, 2001. doi: 10.1201/9781420036060.

Paul A Martin. *Multiple scattering: interaction of time-harmonic waves with N obstacles*. Number 107 in Encyclopedia of Mathematics and its Applications. Cambridge University Press, 2006.

Justin PL McGuinness. *Hydrodynamic optimisation of an array of wave-power devices*. PhD thesis, University College Cork, 2018.

Chiang C Mei, M Stiassnie, and Dick K.-P. Yue. *Theory and applications of ocean surface waves Part 1: Linear aspects*. World Scientific, 2005.

F. Montiel, M. H. Meylan, and S. C. Hawkins. Scattering kernel of an array of floating ice floes: application to water wave transport in the marginal ice zone. *Proceedings of the Royal Society A: Mathematical, Physical and Engineering Sciences*, 480(2282):20230633, 2024. doi: 10.1098/rspa.2023.0633.

Mehdi Neshat, Bradley Alexander, Nataliia Y. Sergiienko, and Markus Wagner. New insights into position optimisation of wave energy converters using hybrid local search. *Swarm and Evolutionary Computation*, 59:100744, 2020. ISSN 2210-6502. doi: https://doi.org/10.1016/j.swevo.2020.100744. URL https://www.sciencedirect.com/science/article/pii/S2210650220303977.

Michel K. Ochi. *Ocean Waves: The Stochastic Approach*. Number 6 in Cambridge Ocean Technology Series. Cambridge University Press, 1998.

Malte A. Peter and Michael H. Meylan. Infinite-depth interaction theory for arbitrary floating bodies applied to wave forcing of ice floes. *Journal of Fluid Mechanics*, 500:145–167, 2004. doi: 10.1017/S0022112003007092.

Willard J Pierson Jr and Lionel Moskowitz. A proposed spectral form for fully developed wind seas based on the similarity theory of SA Kitaigorodskii. *Journal of geophysical research*, 69(24):5181–5190, 1964.

Richard Porter. *Complementary Methods and Bounds in Linear Water Waves*. PhD thesis, University of Bristol, 1995.

Wanan Sheng. Wave energy conversion and hydrodynamics modelling technologies: A review. *Renewable and Sustainable Energy Reviews*, 109:482–498, 2019. ISSN 1364-0321. doi: https://doi.org/10.1016/j.rser.2019.04.030. URL https://www.sciencedirect.com/science/article/pii/S1364032119302424.

Felipe Teixeira-Duarte, Daniel Clemente, Gianmaria Giannini, Paulo Rosa-Santos, and Francisco Taveira-Pinto. Review on layout optimization strategies of offshore parks for wave energy converters. *Renewable and Sustainable Energy Reviews*, 163:112513, 2022. ISSN 1364-0321. doi: https://doi.org/10.1016/j.rser.2022.112513. URL `https://www.sciencedirect.com/science/article/pii/S1364032122004178`.

Jørgen Hals Todalshaug, Gunnar Steinn Ásgeirsson, Eysteinn Hjálmarsson, Jéromine Maillet, Patrik Möller, Pedro Pires, Matthieu Guérinel, and Miguel Lopes. Tank testing of an inherently phase-controlled wave energy converter. *International Journal of Marine Energy*, 15:68–84, 2016. ISSN 2214-1669. doi: https://doi.org/10.1016/j.ijome.2016.04.007. URL `https://www.sciencedirect.com/science/article/pii/S2214166916300182`. Selected Papers from the European Wave and Tidal Energy Conference 2015, Nante, France.

Amélie Têtu, Francesco Ferri, Morten Bech Kramer, and Jørgen Hals Todalshaug. Physical and mathematical modeling of a wave energy converter equipped with a negative spring mechanism for phase control. *Energies*, 11(9), 2018. ISSN 1996-1073. doi: 10.3390/en11092362. URL `https://www.mdpi.com/1996-1073/11/9/2362`.

Amy-Rose Westcott, Luke G. Bennetts, Nataliia Y. Sergiienko, and Benjamin S. Cazzolato. Broadband near-perfect capture of water wave energy by an array of heaving buoy wave energy converters. *Journal of Fluid Mechanics*, 998: A5, 2024. doi: 10.1017/jfm.2024.819.

Ben Wilks and Michael H. Meylan. A numerical comparison of eigenfunction matching and singularity-respecting galerkin approximation methods for linear water wave scattering. *Journal of Marine Science and Engineering*, 13(3), 2025. doi: 10.3390/jmse13030398.

Ben Wilks, Fabien Montiel, and Sarah Wakes. Rainbow reflection and broadband energy absorption of water waves by graded arrays of vertical barriers. *Journal of Fluid Mechanics*, 941, 2022.

W. J. Wiscombe. Improved Mie scattering algorithms. *Appl. Opt.*, 19(9):1505–1509, May 1980. doi: 10.1364/AO.19.001505.

Ronald W. Yeung. Added mass and damping of a vertical cylinder in finite-depth waters. *Applied Ocean Research*, 3 (3):119–133, July 1981. ISSN 0141-1187. doi: 10.1016/0141-1187(81)90101-2.

Xian-tao Zhang, Jian-min Yang, and Long-fei Xiao. An oscillating wave energy converter with nonlinear snap-through power-take-off systems in regular waves. *China Ocean Engineering*, 30(4):565–580, 2016. doi: 10.1007/s13344-016-0035-5.